

Charge pumping in magnetic tunnel junctions: Scattering theory

Jiang Xiao,¹ Gerrit E. W. Bauer,¹ and A. M. Brataas²

¹Kavli Institute of NanoScience, Delft University of Technology, 2628 C.J. Delft, The Netherlands

²Department of Physics, Norwegian University of Science and Technology, NO-7491 Trondheim, Norway
(Dated: February 20, 2024)

We study theoretically the charge transport pumped by magnetization dynamics through epitaxial F/I/F and F/N/I/F magnetic tunnel junctions (F: Ferromagnet, I: Insulator, N: Normal metal). We predict a small but measurable DC pumping voltage under ferromagnetic resonance conditions for collinear magnetization configurations, which may change sign as function of barrier parameters. A much larger AC pumping voltage is expected when the magnetizations are at right angles. Quantum size effects are predicted for an F/N/I/F structure as a function of the normal layer thickness.

A magnetic tunnel junction (MTJ) consists of a thin insulating tunnel barrier (I) that separates two ferromagnetic conducting layers (F) with variable magnetization direction.¹ With a thin normal metal layer inserted next to the barrier, the MTJ is the only magnetoelectronic structure in which quantum size effects on electron transport have been detected experimentally.² More importantly, MTJs based on transition metal alloys and epitaxial MgO barriers^{3,4} are the core elements of the magnetic random-access memory (MRAM) devices⁵ that are operated by the current-induced spin-transfer torque.^{6,7}

It is known that a moving magnetization of a ferromagnet pumps a spin current into an attached conductor.⁸ Spin pumping can be observed indirectly as increased broadening of ferromagnetic resonance (FMR) spectra.⁹ The spin accumulation created by spin pumping can be converted into a voltage signal by an analyzing ferromagnetic contact.¹⁰ This process can be divided into two steps: (1) the dynamical magnetization pumps out a spin current with zero net charge current, (2) the static magnetization (of the analyzing layer) filters the pumped spin current and gives a charge current. In the presence of spin- \uparrow scattering, the spin-pumping magnet can generate a voltage even in an FN bilayer.^{11,12} Spin-pumping by a time-dependent bulk magnetization texture such as a moving domain wall is also transformed into an electric motive force.¹³ Other experiments on spin-pumping induced voltages have also been reported.^{14,15}

Here we present a model study of spin-pumping induced voltages (charge pumping) in MTJs. Since the ferromagnets are separated by tunnel barrier, we cannot use the semiclassical approximations appropriate for metallic structures.^{10,11,16,17} Instead, we present a full quantum mechanical treatment of the currents in the tunnel barrier by scattering theory. The high quality of MgO tunnel junctions and the prominence of quantum oscillations observed in FNIF structures (even for alumina barriers) provide the motivation to concentrate on ballistic structures in which the transverse Bloch vector is conserved during transport. For a typical MTJ under FMR with cone angle $\theta = 5^\circ$ at frequency $f = 20$ GHz, we find a DC pumping voltage of $\hbar\gamma_{\text{cp}}/j \sim 20$ nV for collinear magnetization configurations or AC voltage with amplitude $\nabla_{\text{cp}} \sim 0.25$ V for perpendicular configurations. The magnetization dynamics-induced voltages

could give simple and direct access to transport parameters of high-quality MTJs, such as barrier height, magnetization anisotropies and damping parameters in a non-destructive way. The polarity of the pumping voltage can be changed by engineering the device parameters, etc. An oscillating signal as a function of the thickness of the N spacer leads to Fermi surface calipers that are in tunnel junctions not accessible via the exchange coupling.

We consider a structure shown in Fig. 1 (a), where two semi-infinite F leads (F(L) and F(R)) are connected by an insulating layer (I) of width d and a non-magnetic metal layer (N) of width a . The magnetization direction of F(L)/F(R), $\mathbf{m}_1 = \mathbf{m}_2$ ($j_{\mathbf{m}_1} = j_{\mathbf{m}_2} = 1$), is treated as fixed/free. We disregard any spin accumulation in F, thus treat them as ideal reservoirs in thermal equilibrium. This is allowed when the spin-pumping current is much smaller than the spin- \uparrow rate in the ferromagnet, which is usually a good approximation. The structure reduces to an F/I/F MTJ when $a = 0$. Let A, B, \dots, F be the spin-dependent amplitudes ($A^\uparrow = (A_\parallel^\uparrow; A_\perp^\uparrow)$) at specific points (see Fig. 1) of flux-normalized spinor wave-functions. The scattering states can be expressed in terms of the incoming waves A and F , such as:

$$E = S_{EA}A + S_{EF}F; \quad (1)$$

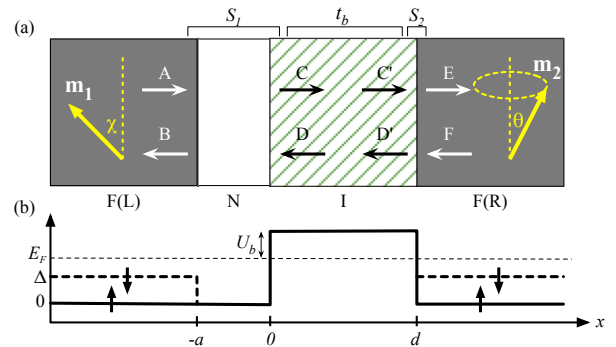


FIG. 1: (Color online) (a): FNIF heterostructure, in which $S_{1,2}$ indicate two different scattering regions. (b): Potential profiles for majority and minority spins in F are shown by solid and dashed lines. The exchange splitting is Δ and the tunnel barrier has height U_b relative to the Fermi energy E_F .

where \hat{S}_{EA} and \hat{S}_{EF} are 2×2 matrices in spin space and can be calculated by concatenating the scattering matrices of region $S_{1,2}$ and of the bulk layer I. To first order of the transmission (t_b) through the bulk I,

$$\hat{S}_{EA} = \hat{t}_2 (1 - \hat{r}_b^0 \hat{r}_2)^{-1} t_b (1 - \hat{r}_1^0 r_b)^{-1} \hat{t}_1; \quad (2)$$

where $\hat{t}_{1,2}/\hat{r}_{1,2}$ are the 2×2 transmission/reflection matrices for $S_{1,2}$ (see Fig. 1), the hatless $t_b=r_b$ are the spin-independent transmission/reflection coefficient for the insulating bulk I. The primed and unprimed version specify the scattering of electrons emitted coming from the left and right, respectively. The reflection coefficient r_b is due to the impurity scattering inside the bulk I, and its magnitude mainly depends on the impurity density in I, especially near the interfaces. All scattering coefficients are matrices in the space of transport channels at the Fermi energy that are labeled by the transverse wave vectors in the leads: $q; q^0$ (the band index is suppressed).

The response to a small applied bias voltage can be written as $J_c = G_c V$ with conductance G_c :

$$G_c = \sum_{q, q^0} g_c(q; q^0) \quad \text{with} \quad g_c = \frac{e^2}{h} \text{Tr} [\hat{S}_{EA} \hat{S}_{EA}^V]; \quad (3)$$

where $\text{Tr} [\quad]$ denotes the spin trace and the summation is over all transverse modes in the leads at the Fermi level.

When the structure is unbiased but the magnetic configuration is time-dependent, a spin current is pumped through the structure.⁸ When the dynamics is slow, $m_{\perp} \ll E_F$, it can be treated by the theory of adiabatic quantum pumping.¹⁸ We consider a situation in which the magnetization (m_2) of one layer precesses with velocity ω around the z -axis with constant cone angle θ , whereas the other magnetization (m_1) is constant (see Fig. 1). We focus on the charge current that accompanies the spin pumping:

$$J_{cp} = \sum_{q, q^0} j_{cp}(q; q^0); \quad (4)$$

$$j_{cp} = \frac{e}{2} \text{Tr} [\text{Im} (\partial \hat{S}_{EA}) \hat{S}_{EA}^V + (\partial \hat{S}_{EF}) \hat{S}_{EF}^V];$$

When a DC current is blocked (open circuit), a voltage bias V_{cp} builds up

$$V_{cp} = G_c^{-1} J_{cp}; \quad (5)$$

The discussion above is valid for general scattering matrices that e. g. include bulk and interface disorders. In order to derive analytical results, we shall make some approximations. First of all, we assume that spin is conserved during the scattering, \hat{t}_i for S_i ($i = 1, 2$, similar for \hat{r}_i) is collinear with m_i .⁸ Expanded in Pauli matrices $\hat{\sigma} = (\hat{\sigma}_x; \hat{\sigma}_y; \hat{\sigma}_z)$, $\hat{t}_i = t_i^+ + t_i^- \hat{\sigma}_z$, with $t_i^\pm = (t_i^\uparrow \mp t_i^\downarrow)/2$. t_i^\pm ($= \uparrow, \downarrow$) is the transmission amplitude for spin-up/down electrons with spin quantization

axes m_i in the scattering region S_i . In the absence of impurities ($r_b = r_b^0 = 0$), Eq. (2) becomes

$$\hat{S}_{EA} = (t_2^+ t_b t_1^+ + t_2^- t_b t_1^- m_1 \cdot m_2) + \hat{\sigma}_z t_2^+ t_b t_1 m_1 + t_2^- t_b t_1 m_2 - i t_2^- t_b t_1 m_1 \cdot m_2; \quad (6)$$

Since all hatless quantities in this equation are still matrices in k -space, such as $t_2^\pm = t_2^\pm(q; q^0)$, the order of $t_2^\pm; t_b; t_1$ as in Eq. (2) should be maintained. The \hat{S}_{EF} term in Eq. (4) may be disregarded, because only the part of \hat{S}_{EF} that depends on both m_1 and m_2 contributes to j_{cp} , and that part is in higher order of t_b .

Another approximation is the free electron approximation tailored for transition metal based ferromagnets.¹⁹ We assume spherical Fermi surfaces for spin-up and spin-down electrons (in both F(L) and F(R)) with Fermi wave-vectors $k_F^\uparrow = \sqrt{2m E_F}/\hbar$ and $k_F^\downarrow = \sqrt{2m (E_F - U_b)}/\hbar$, with an effective electron mass m in F. Electrons in N are assumed to be ideally matched with the majority electrons in F ($k_F = k_F^\uparrow; m_N = m$). Let U_b and $m_b = m$ be the barrier height of and effective mass in the tunnel barrier. The adopted potential profile is shown in Fig. 1(b). We assume the transverse wave-vector q to be conserved ($q = q^0$) by disregarding any impurity or interface roughness scattering, which means the scattering matrices ($t_{1,2}; r_{1,2}; t_b$) are diagonal in k -space. With these approximations, the double summation in Eqs. (3, 4) is replaced by a single integration over transverse wave-vectors. The scattering amplitudes t_i and r_i can be calculated by matching the flux-normalized wave-functions at the interfaces. The transmission coefficient in the barrier bulk is the exponential decay: $t_b = e^{-d}$ with $d = \sqrt{2m_b U_b}/\hbar + q^2$. Then we obtain our main result from Eq. (6):

$$g_c = \frac{e^2}{2h} e^{-2d} [T_1^+ T_2^+ + T_1^- T_2^- m_1 \cdot m_2]; \quad (7a)$$

$$j_{cp} = \frac{e}{2} e^{-2d} [T_1^- m_1 \cdot j_2^{\uparrow\downarrow} (m_2 \cdot m_2) + \text{Im} [t_2^+ t_2^- m_2]; \quad (7b)$$

where $T_i^\pm = j_1^\uparrow j_1^\downarrow + j_1^\downarrow j_1^\uparrow$ is the total transmission probability for scattering region S_i , and $T_i = p_i T_i^\pm = j_1^\uparrow j_1^\downarrow - j_1^\downarrow j_1^\uparrow$ with polarization $p_i = T_i^-/T_i^+$. In Eq. (7b), The term in the square brackets is the transmitted spin pumping current, and $T_1^- m_1$ represents the filtering by the static layer that converts the spin into a charge current.

For an Fe/MgO/FeM TJJ: $k_F^\uparrow = 1.09 \text{ \AA}^{-1}$ and $k_F^\downarrow = 0.42 \text{ \AA}^{-1}$ for Fe,¹⁹ and $U_b \sim 1 \text{ eV}$ and $m_b = m = 0.4$ for MgO.^{3,20} This implies $E_F \sim 4.5 \text{ eV}$, $\theta \sim 38^\circ$ ($\sim 0.85 E_F$, and $U_b \sim 0.25 E_F$ ($t_b \sim 1$ when $U_b > 0.1 E_F$ and $d > 0.5 \text{ nm}$). For an FI/F structure ($a = 0$), both S_1 and S_2 contain only a single F(L)/I (for S_1) or I/F(R) (for S_2) interface. From the potential profile in Fig. 1(b),

$$t_i = t_2 = \frac{2}{k_x + i} \frac{p}{ik_x}; \quad (8)$$

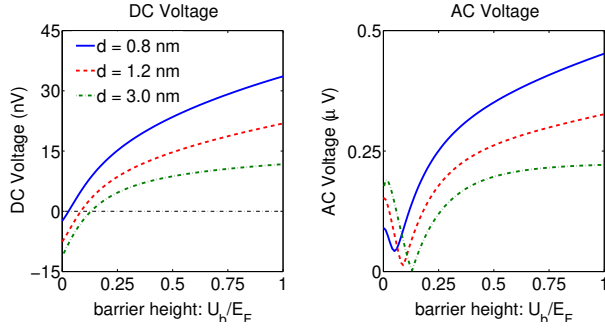


FIG. 2: (Color online) Barrier height (U_b) and width (d) dependence of the pumping voltage. Left: DC. Right: Maximum amplitude of AC voltage.

for $k_x^2 = k_F^2 - q^2 > 0$ and zero otherwise.

If m_2 precesses about an axis that is parallel to m_1 ($\theta = 0$ or 180° , see Fig. 1) $m_1 \cdot m_2 = 0$ and the second term in Eq. (7b) vanishes. The dot product $\mathbf{m}_1 \cdot \mathbf{m}_2 = 2f \sin^2 \theta$ is time-independent, thus generates a DC signal. Let us consider an FIF MTJ with barrier width $d = 0.8$ nm, with m_2 precessing around the z -axis at frequency $f = 20$ GHz with cone angle $\theta = 5^\circ$. We find a DC charge pumping voltage over the F leads $V_{cp} = 15$ nV when m_1 is parallel to the precession axis ($\theta = 0^\circ$) and $V_{cp} = 19$ nV when anti-parallel ($\theta = 180^\circ$).²¹ $|j_{cp}|$ is higher for the anti-parallel configuration simply because its resistance is higher. When the precession cone angle $\theta = 10^\circ$,²² the DC voltage $|j_{cp}| = 60$ nV, similar to a previously measured pumping voltage in a metallic junction.¹²

Fig. 2(a) shows the DC V_{cp} as a function of the barrier height U_b for an FIF structure at $\theta = 5^\circ$ and $f = 20$ GHz. $V_{cp} = G_c^{-1} j_{cp}$ increases as a function of barrier height mainly because $G_c^{-1} j_{cp}$ increases as a function of U_b : From Eq. (7), we have $G_c^{-1} j_{cp} = (T_1 = T_1^+) (j_2 = j_2^+)$ (assume $T_1 T_2 = T_1^+ T_2^+$). The first ratio $T_1 = T_1^+ = p_1 / [(k_x^2 - k_{\#}^2) / (k_x^2 + k_{\#}^2)]$, increases as a function of U_b through (U_b) , whereas second ratio $j_2 = j_2^+ / (k_x^2 - k_{\#}^2) = (k_x^2 + k_{\#}^2)$ is independent of U_b . The pumping voltage therefore increases with U_b (and $1/d$). We also see that V_{cp} decreases when d increases, which can be understood by the following: The effect of the tunnel barrier is to focus the transmission electrons on small q 's due to the exponential decay factor $\exp[-2(qd)]$. Smaller q implies larger kinetic energy normal to the barrier and therefore reduced sensitivity to the spin-dependent potentials. Hence, V_{cp} decreases with barrier width. The lowest curve in Fig. 2(a) is approximately $V_{cp} = G_c^{-1}(q) j_{cp}(q)|_{q=0}$, because for large d the electrons near $q = 0$ completely dominate the transmission. The negative value of V_{cp} in Fig. 2(a) is caused by the negative polarization ($p_1 < 0$) at low barrier height U_b for electrons with small q . V_{cp} remains finite for infinitely high or wide barrier, however, the time to build up this voltage, the RC time (τ_{RC}), goes to infinity due to the exponential growth of the resistance.

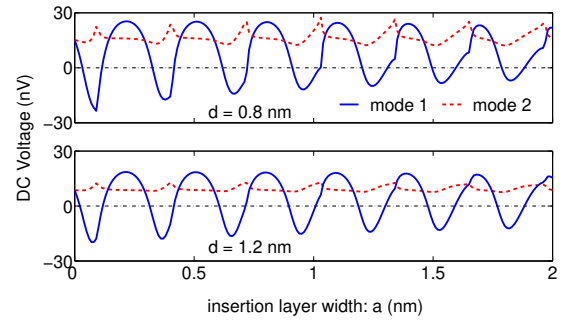


FIG. 3: (Color online) V_{cp} vs. N layer thickness a for FN IF ($U_b = 0.25E_F$).

When m_1 is perpendicular to the precession axis of m_2 , i.e. $\theta = 90^\circ$, the charge pumping voltage oscillates around zero because both dot products in Eq. (7b), $m_1 \cdot m_2 = 2f \sin \theta \cos(2ft)$ and $m_1 \cdot m_2 = 2f \sin \theta \sin(2ft)$, give rise to an AC signal. With $V_{cp} = a m_1 \cdot m_2 + b m_1 \cdot m_2$, where the two components are out of phase by $\pi/2$, the amplitude is given by $V_{cp} = 2f \sin \theta \sqrt{a^2 + b^2}$. An FMR with $\theta = 5^\circ$ and $f = 20$ GHz then gives an AC pumping voltage with amplitude as large as $V_{cp} = 0.25$ V. Fig. 2(b) shows the barrier height dependence of amplitude V_{cp} quite similar to the DC case in Fig. 2(a) and for similar reasons. For a half-metallic junction, the magnitude of the DC pumping voltage V_{cp} can be shown to be bounded by $(\sim 1/2e) \sin^2 \theta$ and AC pumping voltage amplitude V_{cp} must be smaller than $(\sim 1/2e) \sin \theta$, where $\theta = 2f$.

When an N layer of thickness a is inserted, it is interesting to inspect the two different modes, mode 1: FN F and mode 2: FN IF, where F indicates the F layer under FMR. Eq. (7b) applies to mode 1, and applies to mode 2 with subscript 1 and 2 swapped. The N layer forms a quantum well for spin-down electrons that causes the oscillation in the charge pumping voltage as a function of a as shown in Fig. 3. The period of the quantum oscillation due to the N insertion layer is about $\pi/k_F \approx 3\text{Å}$. However, due to the aliasing effect caused by the discrete thickness of the N layer,²³ the observed period should be $\pi/k_F \approx \pi/j$, where j is the thickness of a monolayer. In mode 1, the quantum well formed by the N layer can modulate $T_1(a)$ such that the electrons contributing to the transmission the most have $T_1 > 0$ ($p_1 > 0$) or $T_1 < 0$ ($p_1 < 0$), and thus change the sign of the pumping voltage V_{cp} . On the other hand, there is no sign change in mode 2 because T_2 is independent of a . Similar oscillations could also be found for the amplitude of the AC pumping voltage.

Because the AC voltage is proportional to $\sin \theta$ and DC voltage is proportional to $\sin^2 \theta$, the AC pumping voltage is much larger than the DC counterpart at small θ . However, in order to observe an AC pumping voltage, the time to build up the voltage, the RC time $\tau_{RC} = RC$, has to be shorter than the pumping period, i.e. $\tau_{RC} < 1/f$.

$1/f$. Approximately $\tau_{RC} = (\epsilon_0 \epsilon / 2e^2) e^2 / 2m_b U_b \approx \epsilon_0 \epsilon d / 2e^2$, where ϵ and ϵ_0 are the dielectric constant and electric constant, respectively. A more accurate estimation of the RC time for a typical structure is as follows: the resistance-area (RA) value of the MTJ in our calculation is $RA \approx 3 \text{ m}^2$ for $d = 0.8 \text{ nm}$ ($RA \approx 70 \text{ m}^2$ for $d = 1.2 \text{ nm}$, which is consistent with experimental values.³) The capacitance of an MGO tunnel barrier with $d = 0.8 \text{ nm}$ is calculated by $C = \epsilon_0 \epsilon / d \approx 0.1 \text{ F/m}^2$ ($\epsilon \approx 9.7$ for MGO). Therefore $\tau_{RC} = (RA)(C/A) \approx 0.3 \text{ ps}$ ($1/f \approx 10^3 \text{ ps}$). The electromagnetic response is therefore sufficiently fast to follow the AC pumping signal.

We ignored interface roughness and barrier disorder in the calculation of the pumping voltage. This may be justified by the high quality of epitaxial MGO tunnel barrier.^{3,4} Furthermore, the geometric interface roughness mainly reduces the nominal thickness of the barrier²⁴ which can be taken care of by an effective thickness parameter. Impurity states in the barrier open additional tunneling channels with $U_b^0 < U_b$, which generally increases tunneling but also reduces the spin-dependent effects when spin- $\uparrow\downarrow$ is involved. In general, interface roughness and disorder can be important quantitatively, but have been shown not to qualitatively affect the features predicted by a ballistic model.²⁵ In order to be

quantitatively reliable, the real electronic structure has to be taken into account as well. Both band structure and disorder effects can be taken into account by first-principles electronic structure calculation as demonstrated in for metallic structures.²⁶

Recently, a magnetization-induced electrical voltage of the order of μV was measured for an FIN structure by Mori et al.²⁷ The authors explain their findings by spin pumping, but note that the signal is larger than expected. An FMR generated electric voltage generation up to 100 V was theoretically predicted for such FIN structures.²⁸ Surprisingly, this voltage is much larger than $\sim 1/2 e \hbar / m_b \approx 2e \mu\text{V}$, the maximum "intrinsic" energy scale in spin-pumping theory.

To summarize, a scattering matrix theory is used to calculate the charge pumping voltage for a magnetic multilayer structure. An experimentally accessible charge pumping voltage is found for an FIF MTJ, the pumping voltage can be either DC or AC depending on the magnetization configurations. In FNF structure we find on top of the previously reported oscillating TMR² a charge pumping voltage that oscillates and may change sign with the N layer thickness.

This work has been supported by EC Contract IST-033749 "DynaMax".

- ¹ X. G. Zhang and W. H. Butler, J. of Phys.: Cond. Mat. 15, 1603 (2003). E. Y. Tsybal, O. N. Mryasov, and P. R. LeClair, J. of Phys.: Cond. Mat. 15, 109 (2003).
- ² S. Yuasa, T. Nagahama, and Y. Suzuki, Science 297, 234 (2002).
- ³ S. Yuasa, T. Nagahama, A. Fukushima, Y. Suzuki, and K. Ando, Nature Materials 3, 868 (2004).
- ⁴ S. S. P. Parkin, C. Kaiser, A. Panchula, P. M. Rice, B. Hughes, M. Samant, and S. H. Yang, Nature Materials 3, 862 (2004).
- ⁵ T. Kawahara, R. Takemura, K. Miura, et al., Solid-State Circuits Conference, 2007. ISSCC 2007. Digest of Technical Papers. IEEE Inter. 480, (2007). M. Hosomi, H. Yamagishi, T. Yamamoto, et al., Electron Devices Meeting, 2005. IEDM Technical Digest. IEEE Inter. 459, (2005).
- ⁶ J. C. Slonczewski, J. Magn. Magn. Mater. 159, L1 (1996).
- ⁷ L. Berger, Phys. Rev. B 54, 9353 (1996).
- ⁸ Y. Tserkovnyak, A. Brataas, and G. E. W. Bauer, Phys. Rev. Lett. 88, 117601 (2002).
- ⁹ S. Mizukami, Y. Ando, and T. Miyazaki, Phys. Rev. B 66, 104413 (2002).
- ¹⁰ L. Berger, Phys. Rev. B 59, 11465 (1999).
- ¹¹ X. H. Wang, G. E. W. Bauer, B. J. van Wees, A. Brataas, and Y. Tserkovnyak, Phys. Rev. Lett. 97, 216602 (2006).
- ¹² M. V. Costache, M. Sladkov, S. M. Watts, C. H. van der Wal, and B. J. van Wees, Phys. Rev. Lett. 97, 216603 (2006).
- ¹³ S. E. Barnes and S. Maekawa, Phys. Rev. Lett. 98, 246601 (2007). R. A. Duine, Phys. Rev. B 77, 014409 (2008). W. M. Saslow, Phys. Rev. B 76, 184434 (2007). M. Stamenova, T. N. Todorov, and S. Sanvito, Phys. Rev. B 77, 054439 (2008). S. A. Yang, D. Xiao, and Q. Niu, arXiv:0709.1117v2 (2007). Y. Tserkovnyak and M. Mecklenburg, arXiv:0710.5193 (2007).
- ¹⁴ A. Azevedo, L. H. V. Leao, R. L. Rodriguez-Suarez, A. B. Oliveira, and S. M. Rezende, J. Appl. Phys. 97, 10 (2005).
- ¹⁵ E. Saitoh, M. Ueda, H. Miyajima, and G. Tatara, Appl. Phys. Lett. 88, 182509 (2006).
- ¹⁶ A. Brataas, Y. V. Nazarov, and G. E. W. Bauer, Phys. Rev. Lett. 84, 2481 (2000).
- ¹⁷ Y. Tserkovnyak, A. Brataas, G. E. W. Bauer, and B. I. Halperin, Rev. of Mod. Phys. 77, 1375 (2005).
- ¹⁸ M. Buttiker, H. Thomas, and A. Pretre, Zeit. Phys. B 94, 133 (1994). P. W. Brouwer, Phys. Rev. B 58, R10135 (1998).
- ¹⁹ J. C. Slonczewski, Phys. Rev. B 39, 6995 (1989).
- ²⁰ J. S. Moodera and L. R. Kinder, J. Appl. Phys. 79, 4724 (1996). M. Bowen, V. Cros, F. Petro, A. Fert, C. M. Boubeta, J. L. Costa-Kramer, J. V. Anguita, A. Cebollada, F. Briones, J. M. d. Teresa, et al., Appl. Phys. Lett. 79, 1655 (2001). J. Faure-Vincent, C. Tiusan, C. Belboud, E. Popova, M. Hehn, F. Montaigne, and A. Schuhl, Phys. Rev. Lett. 89, 107206 (2002).
- ²¹ For comparison, the DC voltage for a metallic FNF spin valve under same FMR is $V_{cp} \approx 0.2 \text{ V}$ in our calculation.
- ²² M. V. Costache, S. M. Watts, M. Sladkov, C. H. van der Wal, and B. J. van Wees, Appl. Phys. Lett. 89, 232115 (2006).
- ²³ C. Chappert and J. P. Renard, Europhys. Lett. 15, 553 (1991).
- ²⁴ S. Zhang and P. M. Levy, Euro. Phys. J. B 10, 599 (1999).
- ²⁵ H. Itoh, A. Shibata, T. Kumazaki, J. Inoue, and S. Maekawa, J. Phys. Soc. Jpn. 68, 1632 (1999). J. Mathon and A. Umerski, Phys. Rev. B 60, 1117 (1999). H. Itoh,

- J. Inoue, A. Umerski, and J. Mathon, Phys. Rev. B 68, 174421 (2003). P. X. Xu, V. M. Karpan, K. Xia, M. Zwierzycki, I. Marushchenko, and P. J. Kelly, Phys. Rev. B 73, 180402(R) (2006).
- ²⁶ M. Zwierzycki, Y. Tserkovnyak, P. J. Kelly, A. Brataas, and G. E. W. Bauer, Phys. Rev. B 71, 064420 (2005).
- ²⁷ T. Moriyama, R. Cao, X. Fan, G. Xuan, B. K. Nikolic, Y. Tserkovnyak, J. Kolodzey, and J. Q. Xiao, Phys. Rev. Lett. 100, 067602 (2008).
- ²⁸ S. T. Chui and Z. F. Lin, arXiv:0711.4939v1 (2007).